crystals

MDPI

Article

Effect of Nano-Si_3N_4 on the Mechanical Properties of Cement-Based Materials

Jianping Zhu, Lifei Zhu, Chunhua Feng, Xuemao Guan, Yujiang Sun and Wenyan Zhang *

School of Materials Science and Engineering, Henan Polytechnic University, Jiaozuo 454000, China; jianpingzhu@hpu.edu.cn (J.Z.); zlfhpu@163.com (L.Z.); fengchunhua@hpu.edu.cn (C.F.); guanxuemao@hpu.edu.cn (X.G.); hpusyj@163.com (Y.S.)
* Correspondence: zhangwenyan@hpu.edu.cn

Abstract: In this paper, in order to improve the wear resistance of road cement, nano-Si_3N_4 (NSN) was incorporated into cement, and the effect of NSN on compressive strength and wear resistance of road cement was investigated. The main variable of the experimental investigation was the dosage of NSN. The experimental results showed that the addition of NSN could significantly improve the compressive strength and wear resistance of cement paste. Compared with the reference group, the wear resistance can be improved by 46.5% and the compressive strength of cement paste can be improved by 12.3% when the addition of NSN is 0.16% by weight. In addition, the improvement mechanisms of NSN on cement paste were revealed by hydration heat, XRD, DTA-TG, nanoindentation, nitrogen adsorption, and SEM for microscopic phase tests. Through the microscopic analysis, the addition of NSN can accelerate the hydration reaction and promote the hydration degree, optimize the pore structure, and make the cement paste more compact. Additionally, NSN can improve the performance of the interface transition zone (ITZ) and increase the content of HD C-S-H gel. The action mechanism of NSN is mainly dominated by the surface effect, filling effect, and larger surface energy of NSN thereby improving the mechanical properties of cement-based materials. These research results have guiding significance for the design of the high wear resistance and high compressive strength of cement-based materials.

Keywords: nano-Si_3N_4 (NSN); mechanical properties; compressive strength; wear resistance; reinforcing mechanism

Citation: Zhu, J.; Zhu, L.; Feng, C.; Guan, X.; Sun, Y.; Zhang, W. Effect of Nano-Si_3N_4 on the Mechanical Properties of Cement-Based Materials. *Crystals* **2021**, *11*, 1556. https://doi.org/10.3390/cryst11121556

Academic Editor: Pavel Lukáč

Received: 24 October 2021
Accepted: 10 December 2021
Published: 14 December 2021

1. Introduction

Cement concrete has been widely used in highway, tunnel, airport road, and city road construction because of its many advantages such as high strength, strong bearing capacity, low cost, high-temperature resistance, and other advantages [1,2]. However, because road cement directly bears the impact, vibration, and wear of vehicle load, it needs the property of sufficient wear resistance [3]. Road pavement concrete requires high compressive strength and low tensile strength; however, ordinary concrete cannot meet the requirements of road pavement concrete [4]. Therefore, obtaining road cement with high strength and wear resistance is of constant primary concern. Previous research results have shown that the strength of wear resistance can be affected by the hardness of coarse aggregate [5], the density of cement paste [6,7], and the interfacial bond strength [8]. Fiber can also prevent the development of microcracks and greatly improve the mechanical properties of concrete [9,10]. Some scholars believe that nanomaterials have many unique properties due to the fact of their large specific surface area such as the nucleation effect, the particle filling effect, the surface and interface effects, and the pozzolanic reaction [11,12]. If nanomaterials are applied to road materials, it is expected to significantly improve the mechanical properties of road materials and to have good application prospects [13,14]. By adding different nanomaterials into cement-based materials, it can play a role in physical filling or participating in chemical reactions so as to improve the mechanical properties [15,16]. From

previous research and application of nanomaterials in wear resistant concrete, nano-SiO_2, nano-SiC, nano-TiO_2, nano-ZrO_2, nano-BN, nano-Al_2O_3, and nano-MgO were effective in improving the mechanical properties of cement-based materials [3,17,18]. Han [17] studied the change in mechanical properties of cementitious material with fly ash by adding nano-SiO_2, nano-SiC, and two kinds of nano-admixtures. The results showed that the wear resistance of concrete could be significantly improved and the optimal content of nano-SiO_2 and nano-SiC in concrete was determined to be 2% and 3%. Li [18] investigated the effects of different amounts of nanomaterials on the strength and wear resistance of UHPC, which showed that the UHPC specimens doped with nano-MgO had better strength than the blank samples. Especially when the content of nano-MgO was 0.35%, the compressive strength and flexural strength of 7 days were 1.11 times that of the blank samples, and the wear amount was reduced by 10%. Liu [19] investigated the wear resistance of concretes with surface cracks and found that it could be increased with the addition of silica fume. In a previous study determining why nanomaterials can modify and enhance the mechanical properties of cement-based materials, it was proposed that nanomaterials not only have large specific surface areas and small particle sizes but also to have high chemical reactivity [20,21] which allows for obvious modification effects on the properties of cement-based materials by nanomaterials.

From the above application research, nanomaterials present great potential in improving the mechanical properties of cementitious materials. Nano-Si_3N_4 (NSN) has been studied intensively and have excellent properties, such as superior mechanical properties, high hardness, and strong wear resistance [22], which have been widely applied in the fields of chemical industry, aviation, pharmaceuticals, automobiles, and other fields, especially as a special ceramic material. Zhang and Wang obtained ceramic tool materials with good cutting wear properties by adding NSN [23,24]. It is believed that NSN whiskers, as a kind of reinforcing phase, disperse and distribute in the cement matrix, which play a very good connecting role and achieve the effect of strengthening and toughening [25]. Sun et al. pointed out that NSN can improve the bending strength and wear resistance of ceramics with adding NSN [26]. The crystallization behavior and crystal structure of the polymer could be affected by the addition of NSN particles, thus affecting the properties of the composites. However, there are few reports on the research and application of NSN particles in the field of cement and concrete materials [27–29]. There are still several important issues that are unresolved thus far. For example, can it improve the strength? What is its influence on hardness? How does it affect the wear resistance?

On the one hand, the application of NSN in functional ceramic materials has been widely studied because of its excellent performance. On the other hand, researchers have paid increasing attention to nanoparticles as a substitute component to improve the performance of cement-based materials. As the key performance index of concrete pavement, it is of great significance to study the mechanical properties of concrete pavement. Therefore, this paper mainly investigated the effect of different amounts of NSN on the compressive strength and wear resistance of cementitious materials. To further discuss the mechanism of NSN affecting the cementitious materials, the hydration products and hydration process of cement-based materials were analyzed. In addition, a scanning electron microscope technique, nanoindentation, and nitrogen isotherm adsorption analysis were used to perform the microstructure analysis tests.

2. Experiment

2.1. Materials

The type I Portland cement used in this experiment was provided by Qufu United Cement Company. The chemical composition (by weight) of the cement is given in Table 1. The dispersant was polycarboxylate superplasticizer. The type of nanoparticle used in this study was NSN, white powder, which was produced by Shanghai Macklin Biochemical Company. The density of the NSN was 3.44 kg/m^3, and the average particle size of the NSN was 20 nm. A transmission electron microscope image of the NSN is shown in

Figure 1, displaying that most of the NSN particles were found to be well dispersed. The XRD data compared to its standard PDF card 71-0623 are shown in Figure 2.

Table 1. Chemical composition of the cement (%).

SiO_2	Al_2O_3	Fe_2O_3	CaO	MgO	SO_3	Na_2O	f-CaO	Loss	Cl^-
21.66	4.60	3.30	62.79	2.93	2.40	0.67	0.76	1.36	0.01

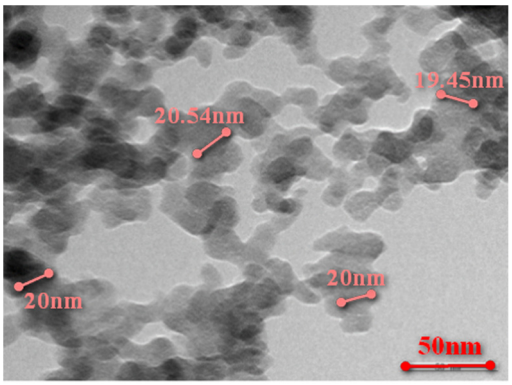

Figure 1. TEM image of the NSN.

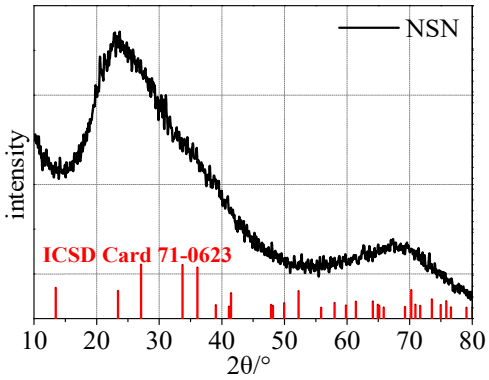

Figure 2. XRD pattern of the NSN.

2.2. Mix Proportion and the Sample Casting

The influence of the NSN on the mechanical properties of cement paste were studied. Ultrasonic dispersion technology and polycarboxylate superplasticizer was applied in this study to ensure the NSN was uniformly dispersed into cementitious materials to obtain the NSN composite cementitious materials. A water reducing agent was added at 0.04% of the weight of the cement as shown in Table 2. The samples were cured in a constant temperature chamber at 20 ± 1 °C with more than 90% relative humidity.

Table 2. Mixture proportions.

Number	Cement (kg/m^3)	Sand (kg/m^3)	Water Reducing Agent (%)	Nano-Si_3N_4 (%)
N_1	240	0	0.04	0.00
N_2	240	0		0.08
N_3	240	0		0.16
N_4	240	0		0.24
N_5	540	1350		0.00
N_6	540	1350		0.08
N_7	540	1350		0.16
N_8	540	1350		0.24

The cement paste samples were manufactured and the influence of the NSN on the compressive strength was examined by varying the dosages of the NSN by 0.00, 0.08, 0.16, and 0.24 wt% (abbreviated as N_1, N_2, N_3, and N_4, respectively). A proportion of the test block was designed as a water-to-cement ratio (w/c) of 0.30 [30]. The water reducing agent was stirred in water for 1 min, then the NSN was added and stirred for 5 min. After that, the stirred solution was ultrasonically dispersed at a power of 250 w for 1 h to prepare for the dispersion liquid. The cement was then added, and the mixture was stirred at a low speed of 500 r/min for 120 s, stopping for 15 s and then stirred at a high speed of 1500 r/min for 120 s in cement paste mixer, then immediately poured into 20 mm × 20 mm × 20 mm molds. After standard curing for 1, 3, 7, and 28 d, the samples were subjected to compressive strength tests. In order to prepare the samples used for the microscopic test, the other samples were soaked in anhydrous ethanol solution for 3 d to terminate hydration. The appropriate number of samples were taken before microscopic testing and dried at 40 °C for 24 h. After drying, the samples were ground into powder and microscopic testing was conducted.

Mortar samples were manufactured and the influence of the NSN on the wear resistance property was examined by varying the dosage of the NSN with 0.00, 0.08, 0.16, and 0.24 wt% (abbreviated as N_5, N_6, N_7, and N_8, respectively). The w/c was designed to be 0.4 and the cement-to-sand ratio (c/s) was 1:2.5 as shown in Table 2. The mortar samples were cast into 150 mm × 150 mm × 150 mm molds, demolded after 1 d, and cured in saturated lime solution for 27 d. After curing, they were dried for 24 h and placed at 60 °C oven for 4 h before wear-resistant experiments.

2.3. Experimental Methods

2.3.1. Compressive Strength

The compressive strengths of cement paste at 1, 3, 7, and 28 d curing ages were examined [1]. In this experiment, the loading rate was set at 0.2 mm/min. The average value of the compressive strength test results was taken from three parallel specimens of cement-based materials.

2.3.2. Wear Resistance

The wear loss per unit area of mortar samples with adding and without adding the NSN were tested using a TM-4 rubber sand wear tester according to JC/T 421-2004. Specimens were ground for 30 revolutions under a load of 200 N, then removed, the floating dust on the surface brushed off, and then they were weighed and the results recorded as the initial mass, M_1. Then, they were ground for another 60 turns, the floating dust on the surface brushed off and weighed and recorded as M_2. The following Equation (1) can be used to calculate the wear loss per unite area:

$$Gc = (M_1 - M_2)/0.0125 \quad (1)$$

In the formula, Gc is the wear loss per unit area (kg/m^2). M_1 is the quantity of before wear and tear (kg); M_2 is the quantity of after wear and tear (kg); 0.0125 is the area of wear (m^2).

2.3.3. Hydration Heat

In order to evaluate the influence of the NSN on the hydration process of cement paste, a TAM Air calorimeter (TA Instruments Co., New Castle, DE, USA) was used to measure the hydration heat change and hydration amount of the cement paste. Samples were prepared at a temperature of 20 °C with a 0.5 w/c ratio [31]. The additional dosage of the NSN corresponded to the experimental design: 0.00, 0.08, 0.16, and 0.24 wt% by the weight of cement. A glass ampoule with 20 mL volume was used by filling 3 g cement powder, and a syringe with 1.5 g water was also prepared. The admix ampoule was first equilibrated in a TAM air calorimeter and the material was separated for 30 min. The

syringe was pushed, and the water in the syringe was injected into the glass ampoule. The hydration reaction of the cement paste then occurred.

2.3.4. XRD Test

In order to analyze the hydration products phase of the cement paste, an XRD test was carried out. Several samples were dried at 60 °C for 24 h. Approximately 2 g of dried sample were ground into powder with agate mortar and passed through an 80 μm square-hole sieve [32]. The sieved powder sample was placed on a glass slide for testing. An X-ray diffractometer with an incident beam of Cu Kα radiation (λ = 1.5418 Å) with a 2θ scanning range of 5–80° was used for this experiment [33]. Powder XRD patterns were collected for the hardened paste at 28 d with the speed of 10°/min.

2.3.5. Differential Thermal Analysis Test

In order to evaluate the hydration degree of the cement paste, differential thermal analysis (TG-DTA, hct-3) was carried out, which was manufactured by Beijing Hengju Scientific Instrument Co., Ltd. In this test, the heating rate was 10 °C/min, and the highest temperature was 1000 °C.

2.3.6. Nanoindentation

The elastic modulus and hardness of the interface transition zone (ITZ) were tested using a Hestron T1-Proier nanoindentation apparatus. A 5–10 mm sample containing an interface region was selected and soaked in an absolute ethyl alcohol solution to terminate hydration. Before the measurement, the specimens were removed from the ethanol solution and dried in a vacuum drying oven at 60 °C for 24 h. The dried surfaces were ground in a sequence of SiC papers (grit #800, #1200, and #2000) and polished in a cloth sequentially with 1 and 0.05 μm diamond sprays. Finally, alcohol and ultrasonic bathing was used to clean the specimen surfaces. Two relatively flat interface areas without visible cracks were selected to conduct a 12 × 8 indentation dot matrix test, and the dot spacing was set to 5 μm. Then, two cement paste areas were used to conduct a 10 × 10 indentation dot matrix test, and the dot spacing was set to 10 μm [34]. The operating conditions of the instrument were as follows: load 5 s to 1000 μN from 0 μN, hold the load for 2 s, and unload 5 s to 0 μN. The abnormal points jumping on the loading curve were deleted in during data processing [35,36].

2.3.7. Nitrogen Isotherm Adsorption Analysis

The pore structure was tested by the nitrogen adsorption method with Tristor3020. After 28 days curing age, the specimens used for the test with the size of 2 mm were prepared. The broken samples of each hydration age were soaked in anhydrous ethanol for 3 d to stop hydration and then dried at 60 °C for 24 h [37].

2.3.8. Microstructural Analysis

In order to analyze the microstructure of the cement-based materials with and without the addition of NSN, a scanning electron microscope (SEM), made by Merlin Compact, was used for this measurement. The specimens with the termination of hydration reaction were prepared according to the same method as the pore structure analysis, and then 20 nm gold powder was sprayed on the samples' surface to make it conductive.

3. Results and Discussion

3.1. Mechanical Properties Results

3.1.1. Influence of the NSN on the Compressive Strength

As described in Section 1, NSN was expected to influence and even modify the macroscopic mechanical properties of the cement-based materials. The influence of different contents of NSN on the compressive strength of cement paste is shown in Figure 3. It was found that the compressive strength of the cement paste specimen increased with

the addition of NSN; when the content of NSN was less than 0.16 wt%, the increase was especially more obvious. Compared with the reference specimen, the compressive strength of specimen with 0.16 wt% NSN at 1, 3, 7, and 28 d increased by 9.20%, 9.46%, 6.35%, and 12.37%, respectively. However, it was also found that when the content of NSN continuously increased to 0.24 wt%, the compressive strength of each age tended to decrease. The reason may be that excessive amounts of NSN cause it to disperse unevenly in the cement paste, causing nanoparticles to agglomerate [38], which affects the strength development of cement-based materials. Therefore, the addition of NSN with 0.16 wt% content by the weight of cement was selected as an optimal mix proportion to improve the compressive strength.

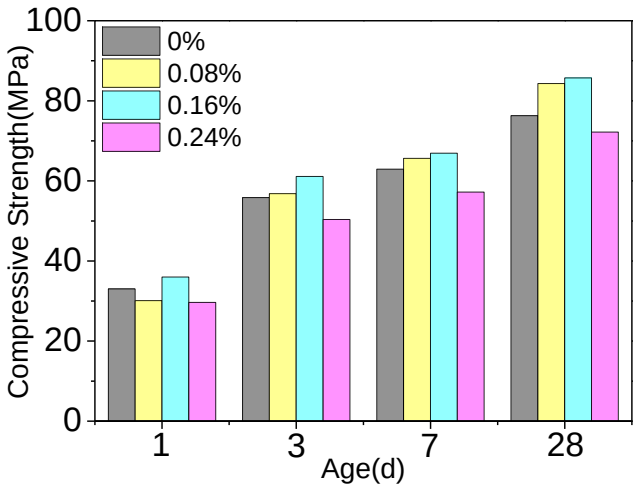

Figure 3. Compressive strength changes of cement paste at 1, 3, 7, and 28 d with different contents of NSN.

3.1.2. Influence of NSN on the Wear Resistance

Effects of samples with different contents of NSN on the wear resistance was shown in Figure 4. The results showed that when the NSN content increased from 0.00 to 0.16 wt%, the wear loss per unit area of the cement mortar test block gradually decreased, that is, the wear resistance of the test block became higher and higher. Compared with the blank specimen, when the content of the NSN was 0.08 wt%, the wear loss per unit area of the specimen was reduced by 32.30%. When the content of NSN was 0.16 wt%, the wear loss per unit area of the specimen decreased by 46.50%. This result means that NSN can effectively improve the wear resistance of cement-based materials. On the one hand, NSN has good strength and wear resistance. On the other hand, NSN, as a nanomaterial, can be effectively filled in the cement paste to promote the hydration reaction process of the paste and improve the compactness of the structure. The compact structure is more conducive to the improvement in compressive strength of cement samples, thus improving the wear resistance [17]. However, when the addition of the content of NSN increased to 0.24 wt%, the wear loss per unit area of the specimen increased obviously. It is supposed that excessive NSN may cause the nanoparticles to agglomerate, inhibit the hydration reaction, reduce the amount of hydration products and the density of cement paste, and then affect the improvement of compressive strength and wear resistance of cement-based materials [18]. Those results showed that the optimal content of NSN into the cement-based materials for increasing the wear resistance was 0.16 wt%.

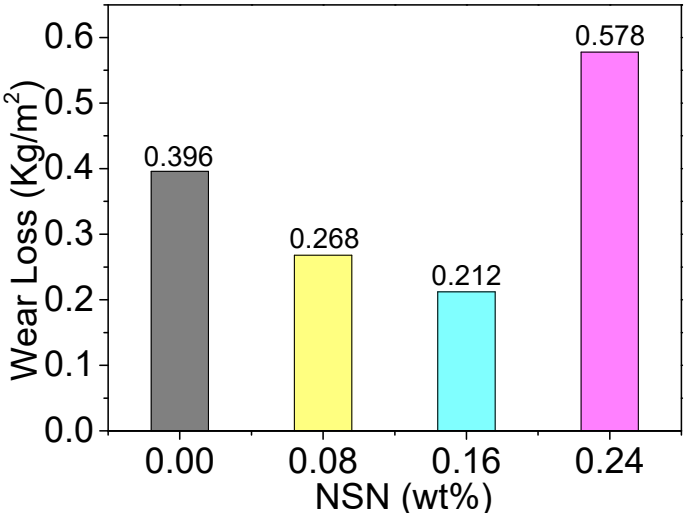

Figure 4. Wear loss per unit area with different contents of NSN.

3.2. Micromechanical Properties Measured by Nanoindentation

The nanoindentation technique can not only test the elastic modulus and hardness of the cement clinker, but it can also test the micromechanical properties for the hydration product and pores of cementitious materials. It can be divided into four sections according to the elastic modulus: 0~13 GPa, 13~26 GPa, 26~39 GPa, and >39 GPa, which represents micropore, low density (LD) C-S-H, high density (HD) C-S-H, and $Ca(OH)_2$, respectively [39,40]. It is generally believed that the indentation modulus of hydration products in cement is not greater than 50 GPa, and if it is greater than this value, it is considered an unhydrated cement clinker and a hydration product [22]. Figure 5a–c shows typical contour maps of an indentation modulus with NSN contents of 0.00, 0.08, and 0.16 wt%, respectively. Research by Xu [41] shows that the dark blue region in Figure 5 represents the ITZ, and it can be seen that the area of the ITZ region decreases obviously with the increase in NSN content, indicating that the addition of NSN can improve the performance of the ITZ. The micromechanical properties of cementitious materials are listed in Table 3. Firstly, the addition of NSN can reduce the content of micropores and increase the average elastic modulus of micropores regions but has little influence on the elastic modulus of LD C-S-H gel. In addition, when the content of NSN was 0.00, 0.08, and 0.16 wt%, the content of HD C-S-H gel was 33.05%, 35.90%, and 51.52% respectively, which shows that the addition of NSN can make LD C-S-H gel easier to be converted into HD C-S-H gel, thus increasing the content of HD C-S-H gel, especially when the content of NSN is 0.16 wt%. These results indicate that the addition of 0.16 wt% NSN can improve the compressive strength and wear resistance due to the generation of HD C-S-H, which will be further demonstrated through other microscopic test analysis.

Table 3. The micromechanical properties of cementitious materials.

	Content/%				Modulus/GPa		
	Pore	LD C-S-H	HD C-S-H	All	Pore	LD C-S-H	HD C-S-H
0.00%	27.97	38.98	33.05	100	5.94	19.93	32.33
0.08%	25.64	38.46	35.90	100	8.71	18.84	32.94
0.16%	12.12	36.36	51.52	100	9.45	19.44	32.66

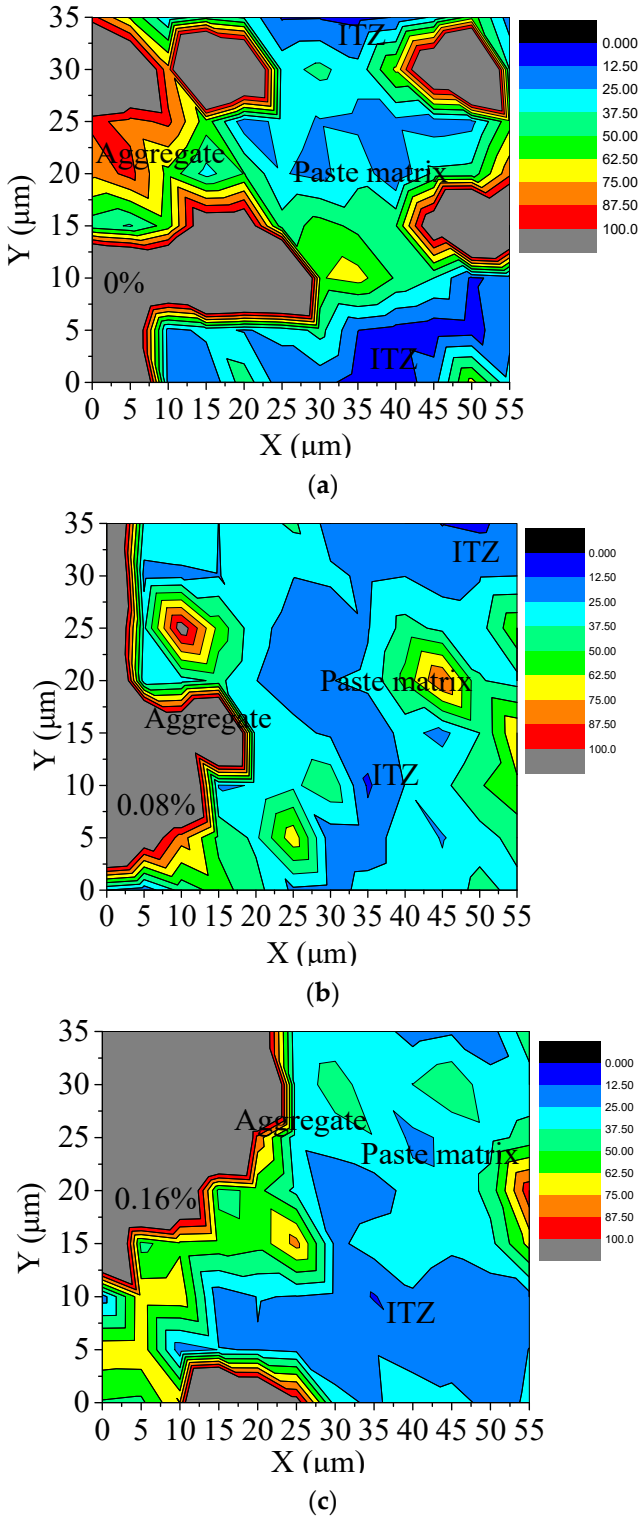

Figure 5. Contour map of the indentation modulus with different content of NSN. (**a**) N5 without NSN. (**b**) N6 with 0.08% content of NSN. (**c**) N7 with 0.16% content of NSN.

3.3. Influence of NSN on the Hydration Process and Hydration Products

3.3.1. Hydration Heat Measurement Result

The early hydration process of cement can be characterized by the amount of heat released during the hydration process or the rate of hydration reaction. These test results were obtained by isothermal calorimetry, and the hydration heat evolution rate and cumu-

lative curves of heat flow versus hydration time of cement paste with different contents of NSN are shown in Figure 6a,b, respectively. The hydration heat values are shown in Table 4.

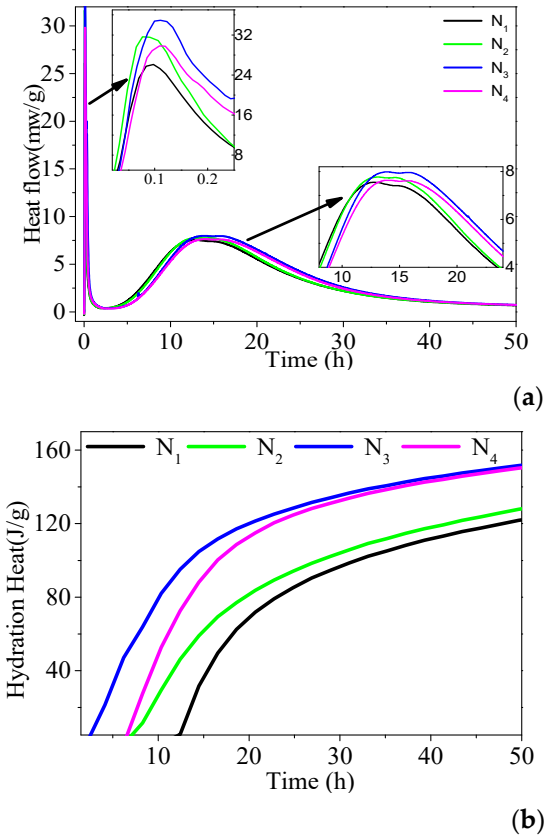

Figure 6. (**a**) Effect of NSN dosage on hydration heat flow; (**b**) effect of NSN dosage on total hydration heat.

Table 4. Peak heat release of hydration heat and accumulated heat release.

Sample	Ending Time of the Induction Period (h)	Peak Value (mW/g)		Total Heat Emission (J/g)
		The First Peak	The Second Peak	
0.00%	2.7	26.11	7.54	129.97
0.08%	3.1	31.63	7.75	136.17
0.16%	3.2	34.94	7.98	156.90
0.24%	3.3	29.81	7.63	156.00

The curves in Figure 6a show a strong and short exothermic peak within the first few minutes (near 0.1 h) when water was added to cement. This was mainly caused by the rapid dissolution of C_3S in cement clinker [42]. This process is called the initial period of hydration reaction. The heat flow peaks in the initial stage were 26.11, 31.63, 34.94, and 29.81 mw/g, respectively. This shows that the addition of NSN provides nucleation sites, thus accelerating the dissolution of cement minerals and rapidly generating a large amount of heat [43]. It was clearly that the hydration induction period of blank group ended in about 2.7 h in Figure 6a. After adding NSN, the hydration induction period was delayed by 3.1–3.3 h. It shows that the addition of NSN could affect the initial hydration reaction; the more NSN that was added, the later the hydration exothermic time appeared before 12 h. Compared with the reference sample N_1, the induction period of other specimens could be slightly prolonged with the addition of NSN particles, and the exothermic rate

of the second hydration heat evolution peak was increased. This was mainly due to the hydration products generated in the initial mixing period adsorbed on the surface of cement particles, which prevents the cement particle from participating in the hydration reaction [44]. When the hydration reaction proceeded for 4 h, a second exothermic peak appeared, and hydration entered an accelerating period.

As can be seen from Table 4, when the contents of NSN were 0.00, 0.08, 0.16, and 0.24 wt%, the second heat flow peaks were 7.54, 7.75, 7.98, and 7.63 mw/g, respectively. This shows that the early hydration of cement could be promoted with the addition of NSN, which leads to the rapid formation of hydration products. However, when the content of NSN was continuously increased to 0.24 wt%, the peak value of the second exothermic peak was reduced to 7.63 mw/g, which indicates that the hydration reaction rate of cement will also decrease due to the excess content of NSN. This was mainly because the agglomerated nanoparticles wrapped the unhydrated cement [42], which hindered the continuation of the hydration reaction.

It can be seen from Figure 6b that the total hydration heat of cement within 72 h was increased with the addition of NSN. The cumulative hydration heat of the sample with 0.00, 0.08, 0.16, and 0.24 wt% NSN was 129.97, 136.17, 156.90, and 156.00 J/g, respectively. The heat release amount increased with the increase in NSN, which indicates that the appropriate addition of NSN can accelerate the heat reaction and increase the thermal evolution at the early age of hydration.

3.3.2. X-Ray Diffraction (XRD) Patterns of Samples

The crystal phases of cement hydration products with different NSN contents at 28 d was determined using the XRD method, and the results are shown in Figure 7. It can be seen that compared with the sample without NSN, the XRD diffraction peak of cement hydration products did not change after adding NSN, indicating that NSN does not generate new hydration products. However, the diffraction peak intensity of CH in the N_3 sample was higher than that of the blank sample N_1, which was due to the fact that a certain amount of NSN could accelerate the hydration reaction of cement as discussed in the Section 3.3.1 hydration heat measurement result. However, when the content of NSN was further increased to 0.24 wt%, the hydration of the C_3S mineral phase in the cement clinker was inhibited, and the formation of CH crystals as a hydration product was delayed due to the agglomeration phenomenon of adding excess nanoparticles [38].

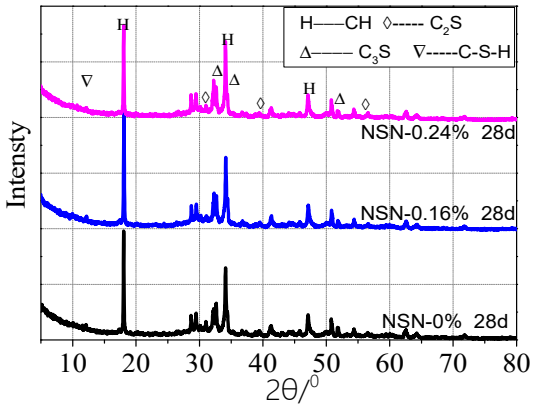

Figure 7. Hydration products of cement-based material with different contents of NSN.

3.4. Scanning Electron Microscopy of Samples

A scanning electron microscope was used to analyze the microstructural characteristics. In order to analyze the morphology of hydration products from designed mixes with NSN, SEM was carried out and the image results are shown in Figure 8. Figure 8a shows that a large amount of loose C-S-H gel was observed in the reference sample N_5, and massive hexagonal platy calcium hydroxide (CH) crystals were present in the pores. In the case of

adding 0.16 wt% NSN (N_7), as shown in Figure 8b, a much denser microstructure with fine needle-shaped AFm was detected. From Figure 8c, it can be found that the hydration structure become looser. According to the literature, the solid-phase volume increased during the chemical reaction [45]. Based on the above pore structure test results, when 0.16 wt% NSN was added, the porosity decreased, and the morphology of the hydration products became much denser. This was mainly due to the effect of proper addition of NSN during the hydration process, which can promote the hydration process, make the structure compact, and leads to a higher compressive strength. However, if the dosage of NSN was more than 0.16 wt%, the agglomeration of nanoparticles may decrease the density of the hydration structure [46].

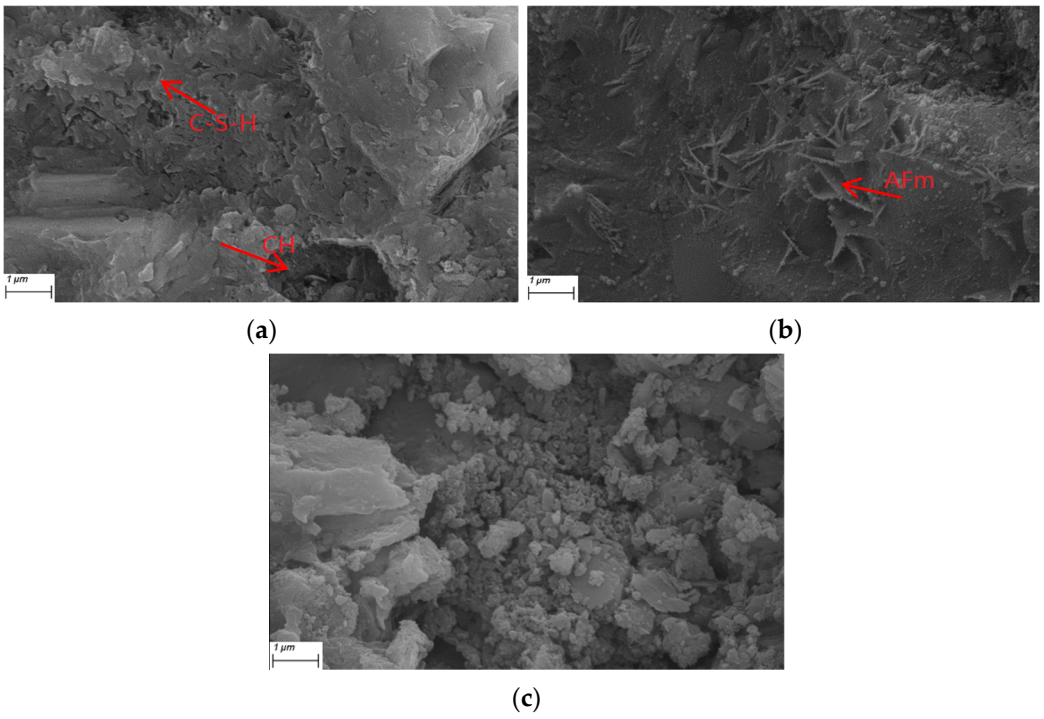

Figure 8. SEM micrographs of the cement-based materials with different contents of NSN at 28 d. (**a**) N5 without NSN. (**b**) N7 with 0.16% content of NSN. (**c**) N8 with 0.24% content of NSN.

3.5. Differential Thermal Analysis (DTA-TG) Result

In order to compare the hydration degree of cement-based materials with different contents of NSN, the data were normalized, and the chemically bound water content was calculated using the data in the temperature range of 105~900 °C. As can be seen from References [47,48], non-chemically bound water can completely evaporate at 105 °C. At 135–150 °C, the C-S-H gel in the slurry lost bound water. At 400~600 °C, the CH crystal in slurry lost crystal water and decomposed. Calcium carbonate decomposed at 600~800 °C.

The content of $Ca(OH)_2$ was calculated based on the Equation (2):

$$M[Ca(OH)_2] = \frac{74}{18} M(H_2O) + \frac{74}{44} M(CO_2) \quad (2)$$

The TG test result and the derived DTA curve of cement-based materials with different NSN contents at 28 d are presented in Figure 9. The TG curve reveals the continuous weight loss of cement-based materials with different NSN contents with the increase in temperature. The main endothermic peaks in the DTA curve appeared at 105, 480, and 660 °C. The endothermic peak at approximately 105 °C was caused by the evaporation of the free water and the dehydration of C-S-H and AFt. The peak at approximately 170 °C corresponded to the decomposition of the AFm phase [38]. The peak at approximately

480 °C represents the decomposition of $Ca(OH)_2$. The peak at approximately 660 °C was due to the decomposition of $CaCO_3$. The results show that when the contents of NSN were 0.00, 0.16, and 0.24 wt%, the mass losses caused by $Ca(OH)_2$ crystal were 1.86%, 2.02%, and 1.87%, respectively. As was expected, the thermal weight-loss percentage of $Ca(OH)_2$ crystal decomposition in the N_3 paste sample was higher than that in other samples. The mass losses caused by the $CaCO_3$ crystals were 1.30%, 1.11%, and 1.05%, respectively. According to Formula (2), the total $Ca(OH)_2$ contents of N_1, N_3, and N_4 were 9.87%, 10.17%, and 9.45%, respectively.

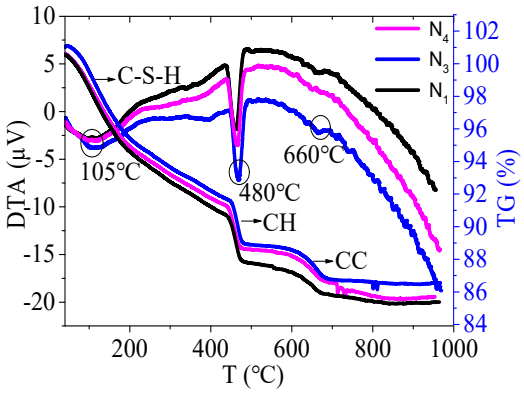

Figure 9. The TG-DTA curves of the cement-based materials with different contents of NSN.

By comparing the weight loss of cement paste with different NSN contents at 28 d of hydration, the specimen with 0.16 wt% NSN showed the highest weight loss, which indicates that the $Ca(OH)_2$ crystal content in cement paste was the highest, the degree of cement hydration was higher, and the hydration was more complete. At the same time, the TG and DTA curves trended in the same direction, indicating that no new hydration products were generated, which is consistent with the XRD analysis results. With the increase iz NSN, the degree of hydration decreases, indicating that the optimal amount of 0.16 wt%. This result is consistent with the results of the XRD analysis and mechanical property results.

3.6. Microstructural Change in the Sample Incorporating NSN

As a type of porous material, many properties of cement-based materials are directly related to pore structure with different pore sizes, ranging from nanometers to millimeters [37]. Therefore, the analysis of pore structure has always been the focus of attention. After hydration and hardening of cement-based materials, pore structure is an important factor that affects mechanical properties. The pore diameters of hardened cement paste can be divided into four categories [49] in which macropores have a more significant influence on mechanical strength [15]. The pore size distribution and cumulative pore volume curves were measured using the Barrette Joyner Halenda (BJH) method, based on the principle of capillary condensation and equivalent volume substitution.

The pore structure and pore size distribution results are given in Figure 10. The peak value of the most probable pore size appears at 3.3 nm. When the content of NSN was 0.16%, the most probable pore size had a minimum value approximately 10 nm. The cumulative pore volume of samples N_5 and N_8 were significantly higher than that of sample N_7 with 0.16 wt% NSN, which indicates that the appropriate content of NSN can reduce the porosity, improve the density of the cement paste, and then improve the mechanical properties of the sample. This result corresponds to the results of compressive strength test and wear resistance test.

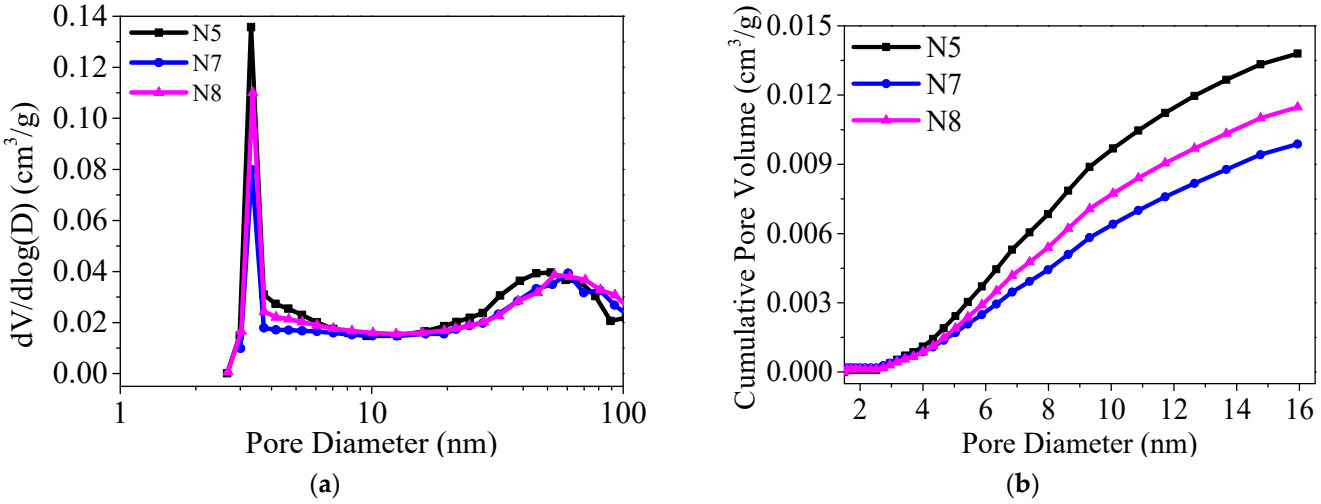

Figure 10. Cumulative intrusion curves (**a**) and pore size distribution (**b**) of cement-based materials doped with 0, 0.16, and 0.24 wt% NSN.

4. Discussion

The results from the experimental and microscopic test analyses were utilized to evaluate the mechanical properties and investigate the microstructural change. The addition of NSN could effectively improve the compressive strength and wear resistance. Through the micromechanical property analysis, it was suggested that improvement of the mechanical properties with 0.16 wt% NSN was due to the generation of HD C-S-H during the hydration process. The macro-properties of cementitious materials are closely related to the structure of hydration products (mainly C-S-H) at the nanoscale. In this study, NSN particles, with a high surface area, can accelerate the heat reaction and increase the thermal evolution at the early age of hydration. NSN can play a role in the crystal nucleus, which can rapidly nucleate and attract cement more $Ca(OH)_2$ in the secondary hydration reaction produces more C-S-H gel and ettringite crystals. The C-S-H is a compound that is the main product of cement hydration and a major factor in the strength of cement and all cement-based products. When the content of NSN was 0.16 wt%, the content of HD C-S-H gel was 51.52%, which was higher than other samples. The SEM results also confirmed the previous research findings on the mechanical properties and show that in the sample with 0.16% NSN, AFm was produced in comparison to the reference sample and sample with 0.24%NSN, which is positive for improving the mechanical properties. The SEM images illustrate that with the addition of NSN, the texture became much denser and more compact. The microstructural change was further demonstrated by the pore volume results measured using the BJH method. The cumulative pore volume of sample N_7 with 0.16 wt% NSN presented the lowest value, which is positive for improving the mechanical properties of cementitious materials.

5. Conclusions

In this paper, the effect of NSN on the mechanical properties of cement-based materials was investigated including compressive strength and wear resistance. Ultrasonic dispersion technology and polycarboxylate superplasticizer was applied in this research to ensure NSN was uniformly dispersed into cementitious materials. The results showed that the addition of NSN had an obvious effect on improving the compressive strength and wear resistance, and when the content of NSN increased from 0.00% to 0.24% by the weight of cement, the compressive strength and wear resistance of cement-based material showed a trend of first increasing and then decreasing. The NSN additives enhanced the compressive strength by 12.3% and the wear resistance of cement-based materials 46.5% when the optimal addition was 0.16 wt%.

Furthermore, the hydration process and microstructure were also discussed through a series of experimental tests. The addition of NSN mainly plays a role in providing nucleation sites, which can accelerate the dissolution of cement minerals and rapidly generate a large amount of heat. With the increase in the content of NSN content, the rate of hydration heat at early ages was promoted, and total heat released was increased. The addition of NSN accelerated the hydration of cement-based materials, resulting in a denser microstructure. The micro-analyses (i.e., XRD, SEM, nanoindentation, and DTA-TG) showed that a suitable addition of NSN compacted the microstructure of cementitious material and promoted the formation of hydration products. There were no new phases formed with the addition of NSN, but too much NSN may hinder the hydration of cement due to the agglomeration phenomenon of adding excess nanoparticles. An appreciating amount of NSN 0.16 wt% could increase hydration products, resulting in a more compact structure and higher performance of the ITZ, thus resulting in a higher compressive strength and wear resistance of cement-based materials.

According to this research, NSN could have a positive effect on cement-based material, and the addition of NSN may have potential value for the further study of cement-based materials.

Author Contributions: Data curation, J.Z., L.Z. and Y.S.; Investigation, X.G.; Supervision, J.Z.; Writing—original draft, J.Z. and C.F.; Writing—review & editing, W.Z. All authors have read and agreed to the published version of the manuscript.

Funding: This work was financially supported by the National Natural Science Foundation of China (51908198, 51872137), the College Students' Innovative Entrepreneurial Training Plan Program (201910460031), the China Postdoctoral Science Foundation (2018M632774), and the Henan Outstanding Foreign Scientists' Workroom (GZS2021003).

Informed Consent Statement: Informed consent was obtained from all subjects involved in the study.

Conflicts of Interest: The authors declare no conflict of interest.

References

1. Zhu, J.; Li, G.; Feng, C.; Wang, L.; Zhang, W. Effect of Delaminated MXene (Ti_3C_2) on the Performance of Cement Paste. *J. Nanomater.* **2019**, *10*, 3074206. [CrossRef]
2. Zhu, J.; Yang, K.; Chen, Y.; Fan, G.; Zhang, L.; Guo, B.; Guan, X.; Zhao, R. Revealing the substitution preference of zinc in ordinary Portland cement clinker phases: A study from experiments and DFT calculations. *J. Hazard. Mater.* **2021**, *409*, 124504. [CrossRef]
3. Zou, C. Study on Design, Performance and Mechanism of Nano Modified Concrete Pavement Materials. Master's Thesis, Changsha University of Science and Technology, Changsha, China, 1 April 2016.
4. Qin, X.; Li, X.; Cai, X. The applicability of alkaline-resistant glass fiber in cement mortar of road pavement: Corrosion mechanism and performance analysis. *Int. J. Pavement Res. Technol.* **2017**, *10*, 536–544.
5. Kumar, S.; Gupta, R.C.; Shrivastava, S. Strength, abrasion and permeability studies on cement concrete containing quartz sandstone coarse aggregates. *Constr. Build. Mater.* **2016**, *125*, 884–891. [CrossRef]
6. Cai, X.; He, Z.; Tang, S.; Chen, X. Abrasion erosion characteristics of concrete made with moderate heat Portland cement, fly ash and silica fume using sandblasting test. *Constr. Build. Mater.* **2016**, *127*, 804–814. [CrossRef]
7. Popek, M.; Sadowski, Ł.; Szymanowski, J. Abrasion Resistance of Concrete Containing Selected Mineral Powders. *Procedia Eng.* **2016**, *153*, 617–622. [CrossRef]
8. He, Z.; Chen, X.; Cai, X. Influence and mechanism of micro/nano-mineral admixtures on the abrasion resistance of concrete. *Constr. Build. Mater.* **2019**, *197*, 91–98. [CrossRef]
9. Ates, A. Mechanical properties of sandy soils reinforced with cement and randomly distributed glass fibers. *Compos. Part B Eng.* **2016**, *96*, 295–304. [CrossRef]
10. Fathi, H.; Lameie, T.; Maleki, M.; Yazdani, R. Simultaneous effects of fiber and glass on the mechanical properties of self-compacting concrete. *Constr. Build. Mater.* **2017**, *133*, 443–449. [CrossRef]
11. Gao, Y.; He, B.; Li, Y.; Tang, J.; Qu, L. Effects of nano-particles on improvement in wear resistance and drying shrinkage of road fly ash concrete. *Constr. Build. Mater.* **2017**, *151*, 228–235. [CrossRef]
12. Wang, D.; Zhang, W.; Ruan, Y.; Yu, X.; Han, B. Enhancements and mechanisms of nanoparticles on wear resistance and chloride penetration resistance of reactive powder concrete. *Constr. Build. Mater.* **2018**, *189*, 487–497. [CrossRef]
13. Zhang, R.; Cheng, X.; Hou, P.; Ye, Z. Influences of nano-TiO_2 on the properties of cement-based materials: Hydration and drying shrinkage. *Constr. Build. Mater.* **2015**, *81*, 35–41. [CrossRef]
14. Gao, Y.; He, B.; Zou, C. Effect and Mechanism of Nano-particles on Wear Resistance of Road Fly Ash Concrete. *Bull. Chin. Ceramic. Soc.* **2018**, *37*, 441–448.

15. Wang, M.J.; Li, H.D.; Zeng, Q.; Chang, Q.F.; Wang, X.S. Effects of nanoclay addition on the permeability and mechanical properties of ultra high toughness cementitious composites. *J. Zhejiang Univ.-Sci. A* **2021**, *21*, 992–1007. [CrossRef]
16. Wang, B.; Fan, C. Comparative Study on Dispersion of Carbon Nanofibers and Enhancement on Mechanical Property and Microstructure in Cement Composites. *J. Nanosci. Nanotechnol.* **2020**, *20*, 113–120. [CrossRef] [PubMed]
17. Han, L.Y. Wear Resistance and Chloride Penetration Resistance of Nano Cement-Base Composites. Master's Thesis, Dalian University of Technology, Dalian, China, 2018.
18. Li, S.X.; Gao, X.J. Effect of nano Al_2O_3 and MgO on abrasion resistance and mechanism of ultra-high performance concrete. *Surf. Technol.* **2018**, *47*, 123–130.
19. Liu, Y.W. Improving the abrasion resistance of hydraulic-concrete containing surface crack by adding silica fume. *Constr. Build. Mater.* **2017**, *21*, 972–977. [CrossRef]
20. Gintautas, S.; Ekaterina, K.; Rostislav, D.; Jakub, H. Hydration and Microstructure of Nano Modified Cement Paste. *Solid State Phenom.* **2021**, *6104*, 9–14.
21. Ying, K.; Yang, S.; Meng, T.; Li, Y. Effect of Nano Compound Addition on the Properties and Microstructure of Cement Mortar with Mixed Fine Recycled Aggregate. *IOP Conf. Ser. Earth Environ. Sci.* **2021**, *719*, 022074. [CrossRef]
22. Liu, X.Z. The Preparation and Microstructure Analysis of Nanoscale Silicon Nitride Podwer. Master's Thesis, Northwest Agriculture and Forestry University, Xianyang, China, 2018.
23. Zhang, Y.B. Study on the Graphene/Silicon Nitride Based Composite Ceramic Tools and Their Friction and Wear Properties. Master's Thesis, Qilu University of Technology, Jinan, China, 2017.
24. Wang, J.H. Study on cutting performance and its extended application of coated silicon nitride cutting tool. *Guangdong Univ. Technol.* **2014**, 9–10. [CrossRef]
25. Huang, L. Effect of Carbon Nanotubes and Si_3N_4 Whiskers on Microstructure and Properities of Mo_2FeB_2-Based Cermets. Ph.D. Thesis, Wuhan University of Science and Technology, Wuhan, China, 2019.
26. Sun, Y.G.; He, S.L.; Liu, R.A.; Jin, H.; Yang, W.L.; Zhang, Y.H. Preparation and Application of Silicon Nitride Ceramics. *China Ceram. Ind.* **2016**, *23*, 31–34.
27. Yin, H.; Zhu, J.; Guan, X.; Yang, Z.; Zhu, Y.; Zhao, H.; Zhang, Z.; Zhou, A.; Zhang, X.; Feng, C.; et al. Effect of MXene (Nano-Ti_3C_2) on Early-Age Hydration of Cement Paste. *J. Nanomater.* **2015**, *16*, 147. [CrossRef]
28. Lv, S.; Ma, Y.; Qiu, C.; Sun, T.; Liu, J.; Zhou, Q. Effect of graphene oxide nanosheets of microstructure and mechanical properties of cement composites. *Constr. Build. Mater.* **2013**, *49*, 121–127. [CrossRef]
29. Han, B.; Wang, Z.; Zeng, S.; Zhou, D.; Yu, X.; Cui, X.; Ou, J. Properties and modification mechanisms of nano-zirconia filled reactive powder concrete. *Constr. Build. Mater.* **2017**, *141*, 426–434. [CrossRef]
30. Corinaldesi, V.; Nardinocchi, A. Influence of type of fibers on the properties of high performance cement-based composites. *Constr. Build. Mater.* **2016**, *107*, 321–331. [CrossRef]
31. Feng, Y.; Kero, J.; Yang, Q.; Chen, Q.; Engström, F.; Samuelsson, C.; Qi, C. Mechanical Activation of Granulated Copper Slag and Its Influence on Hydration Heat and Compressive Strength of Blended Cement. *Materials* **2019**, *12*, 772. [CrossRef]
32. Zhang, F.L. Effect of Nanoparticle on Mechanical Properties of Cement-Based Materials and Its Mechanism. Master's Thesis, Harbin Institute of Technology, Harbin, China, 2016.
33. Zhao, R.; Zhang, L.; Guo, B.; Chen, Y.; Fan, G.; Jin, Z.; Guan, X.; Zhu, J. Unveiling substitution preference of chromium ions in sulphoaluminate cement clinker phases. *Compos. Part B Eng.* **2021**, *222*, 109092. [CrossRef]
34. Gao, X. Analysis of properties of cement-based materials by nanoindentation technique. Master's Thesis, Institute of Highway Science, Ministry of Communications, Beijing, China, 2014.
35. Xu, J.; Wang, X.Z. Effect of nano-silica modification on interfacial transition zone in concrete and its multiscale modelling. *J. Chin. Ceram. Soc.* **2018**, *46*, 1053–1058.
36. Xu, S.; Feng, Y.; Liu, J.; Zeng, Q.; Peng, Y. Microfracture Characterization of Cement Paste at Early Age by Indentation Test. *J. Mater. Civ. Eng.* **2018**, *30*, 04018110. [CrossRef]
37. Zhao, L.; Guo, X.; Liu, Y.; Zhao, Y.; Chen, Z.; Zhang, Y.; Guo, L.; Shu, X.; Liu, J. Hydration kinetics, pore structure, 3D network calcium silicate hydrate, and mechanical behavior of graphene oxide reinforced cement composites. *Constr. Build. Mater.* **2018**, *190*, 150–163. [CrossRef]
38. Zhu, S.; Wang, G.; Deng, J.; Liu, F.; Xiao, M. Effect of Nano-TiO_2 Dispersibility on the Mechanics, Hydration Degree and Microscopic Properties of Cement Paste. *J. Build. Mater.* **2021**, 1–11. Available online: https://kns.cnki.net/kcms/detail/31.1764.TU.20210827.0842.002.html (accessed on 24 October 2021).
39. Chen, X.; Hou, D.; Han, Y.; Ding, X.; Hua, P. Clustering analysis of grid nanoindentation data for cementitious materials. *J. Mater. Sci.* **2021**, *56*, 12238–12255. [CrossRef]
40. Ying, J.; Zhang, X.; Jiang, Z.; Huang, Y. On Phase Identification of Hardened Cement Pastes by Combined Nanoindentation and Mercury Intrusion Method. *Materials* **2021**, *14*, 3349. [CrossRef]
41. Xu, J.; Wang, B.; Zuo, J. Modification effects of nanosilica on the interfacial transition zone in concrete: A multiscale approach. *Cem. Concr. Compos.* **2017**, *81*, 1–10. [CrossRef]
42. Yang, Z.; He, R.; Tan, Y.; Chen, H.; Cao, D. Air pore structure, strength and frost resistance of air-entrained mortar with different dosage of nano-SiO_2 hydrosol. *Constr. Build. Mater.* **2021**, *308*, 125096. [CrossRef]

43. Karpova, E.; Skripkiūnas, G.; Barauskas, I.; Barauskienė, I.; Hodul, J. Influence of carbon nanotubes and polycarboxylate superplasticiser on the Portland cement hydration process. *Constr. Build. Mater.* **2021**, *304*, 124648. [CrossRef]
44. Zhang, Y.R.; Kong, X.M. Correlations of the dispersing capability of NSF and PCE types of superplasticizer and their impacts on cement hydration with the adsorption in fresh cement pastes. *Cem. Concr. Res.* **2015**, *69*, 1–9. [CrossRef]
45. Shao, Q.; Zheng, K.; Zhou, X.; Zhou, J.; Zeng, X. Enhancement of nano-alumina on long-term strength of Portland cement and the relation to its influences on compositional and microstructural aspects. *Cem. Concr. Compos.* **2019**, *98*, 39–48. [CrossRef]
46. Li, G.S.; Feng, C.H.; Zhu, L.F.; He, G.Y.; Hou, H.H.; Xia, R.J.; Gao, G.; Guan, X.M.; Zhu, J.P. Effect of nano-TiN on the performance of fly ash cement. *J. Chin. Ceram. Soc.* **2018**, *37*, 4072–4076.
47. Meng, S.; Ouyang, X.; Fu, J.; Niu, Y.; Ma, Y. The role of graphene/graphene oxide in cement hydration. *Nanotechnol. Rev.* **2021**, *10*, 768–778. [CrossRef]
48. Wu, Z.; Shi, C.; Khayat, K.H.; Wan, S. Effects of different nanomaterials on hardening and performance of ultra-high strength concrete (UHSC). *Cem. Concr. Compos.* **2016**, *70*, 24–34. [CrossRef]
49. Fernandes, R.G.; Reis, R.M.; Tobar, R.R.; Zanotto, E.D.; Ferreira, E.B. Simulation and experimental study of the particle size distribution and pore effect on the crystallization of glass powders. *Acta Mater.* **2019**, *175*, 130–139. [CrossRef]